

UniDrive-WM: Unified Understanding, Planning and Generation World Model For Autonomous Driving

Zhexiao Xiong^{1,2*} Xin Ye¹ Burhan Yaman Sheng Cheng³
 Yiren Lu^{1,4} Jingru Luo¹ Nathan Jacobs² Liu Ren¹

¹ Bosch Research North America & Bosch Center for Artificial Intelligence (BCAI)

² Washington University in St. Louis ³ Arizona State University ⁴ Case Western Reserve University

Abstract

World models have become central to autonomous driving, where accurate scene understanding and future prediction are crucial for safe control. Recent work has explored using vision-language models (VLMs) for planning, yet existing approaches typically treat perception, prediction, and planning as separate modules. We propose UniDrive-WM, a unified VLM-based world model that jointly performs driving-scene understanding, trajectory planning, and trajectory-conditioned future image generation within a single architecture. UniDrive-WM’s trajectory planner predicts a future trajectory, which conditions a VLM-based image generator to produce plausible future frames. These predictions provide additional supervisory signals that enhance scene understanding and iteratively refine trajectory generation. We further compare discrete and continuous output representations for future image prediction, analyzing their influence on downstream driving performance. Experiments on the challenging Bench2Drive benchmark show that UniDrive-WM produces high-fidelity future images and improves planning performance by 5.9% in L2 trajectory error and 9.2% in collision rate over the previous best method. These results demonstrate the advantages of tightly integrating VLM-driven reasoning, planning, and generative world modeling for autonomous driving. The project page is available at <https://unidrive-wm.github.io/UniDrive-WM/>.

1. Introduction

Recent progress in multimodal large language models (MLLMs) has been propelled by the strong perception, reasoning, and instruction-following capabilities of vision-language models (VLMs). In parallel, visual generation has advanced along two complementary lines: au-

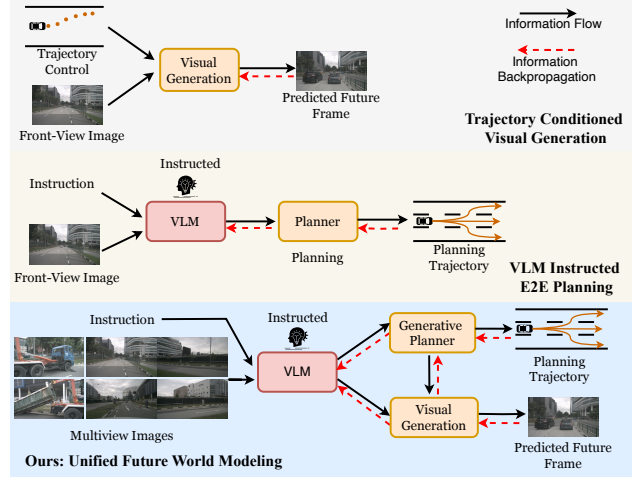


Figure 1. Top: trajectory-conditioned visual generation. Middle: VLM Instructed E2E Planning. Bottom: our unified future world modeling method. Compared with conditioned future image generation models and VLM-Instructed planning method, our framework establishes the connection between the reasoning, action and visual generation space via joint VLM-guided trajectory planner and future frame generation.

toregressive (AR) token prediction and diffusion-based continuous generation—enabling high-fidelity image synthesis across diverse tasks. Motivated by these trends, a growing body of *unified* models seeks to couple understanding and generation within a single VLM, allowing the system to “think and generate” in a shared semantic space [4, 21, 39].

In autonomous driving, world models [25, 49, 49] are typically defined as learned models that infer a latent representation of the current scene and predict future states conditioned on actions, ideally enabling robust planning and control. While several VLM-based approaches have been explored, many rely on text-only intermediates, first producing natural-language descriptions of future trajectories or scenes, and then invoking a separate stage to decode tra-

*Work was done during internship at Bosch Research North America.

jectories or render images. This pipeline introduces an information bottleneck: rich visual–geometric cues are abstracted into text, incurring inevitable loss and compounding errors across stages. Meanwhile, generative models can generate visually plausible frames, but they typically lack explicit state estimation and reasoning. In particular, they do not maintain structured representations of the scene and can not reliably condition on multi-view cues or high-level instructions, which provides no differentiable bridge to the action space for verifiable planning. Consequently, they struggle to answer causal queries (e.g., “what if the pedestrian accelerates?”), to enforce safety constraints, or to propagate plan-consistent signals back into perception. In reality, a driver’s cognition is inherently joint: perceive the current scene, anticipate the future trajectory, and imagine the next visual scene. This motivates a unified formulation in which understanding, planning, and visual prediction are learned end-to-end within a single VLM framework, allowing information to flow bidirectionally between reasoning, action, and generation.

We present **UniDrive-WM**, a unified world model that *jointly* performs scene understanding, trajectory planning, and future image generation within a VLM-centric architecture. As illustrated in Fig. 1, multi-view observations, temporal history, and perception cues (e.g., subject bounding boxes) are encoded and projected into an LLM reasoning space. A trajectory planner then produces a differentiable latent distribution over waypoints, bridging the reasoning (language–vision) space and the numeric action space. Conditioning on the predicted trajectory, UniDrive-WM further performs *trajectory-conditioned* future image prediction via two complementary designs: (i) a discrete AR pathway that expands the visual codebook and detokenizes with MoVQGAN, and (ii) an AR+diffusion pathway that predicts continuous latent features with a flow-matching objective before pixel decoding. This design alleviates text-only bottlenecks and enables bidirectional coupling—both information flow and gradient flow—between reasoning, action, and generation. Extensive experiments on the challenging Bench2Drive dataset show that UniDrive-WM generates high-fidelity future image frames and outperforms counterpart methods on planning tasks across both open-loop and closed-loop metrics.

Our main contributions are summarized as follows:

- We present *UniDrive-WM*, a unified vision–language world model (VLM) that seamlessly integrates scene understanding, trajectory planning, and future image generation, enabling direct visual reasoning from spatio-temporal observations.
- We develop and analyze two complementary decoding paradigms for trajectory-conditioned future image prediction: a *discrete* autoregressive (AR) pathway and a *continuous* AR+diffusion pathway, revealing their respective

advantages and trade-offs for autonomous driving.

- Extensive experiments demonstrate that our unified framework achieves high-fidelity, planning-conditioned visual generation and significantly improves both planning accuracy and perception performance on standard driving benchmarks, verifying the effectiveness of the proposed unified framework.

2. Related Works

World Models for Autonomous Driving. The commonly acceptable description of world models is understanding the current state and predicting the future state. For autonomous driving task, recent world modeling based methods aim to infer the ego status and dynamic environments from past observations to enable future planning and prediction, reducing the human control in the autonomous driving systems. Existing methods can be broadly categorized by their output modality: some focus on visual scene generation [8, 9, 11, 42], others emphasize future trajectory planning [7, 24], while several works address 3D scene reconstruction in the form of occupancy [30, 34], LiDAR [37, 51], or point clouds [43, 44]. However, most of these approaches focus on a single prediction modality. In contrast, our model jointly performs trajectory planning and future image generation within a unified world-model framework, coupling planned motion with predicted visual futures under a shared VLM backbone.

Unified Image Understanding and Generation. Recent studies have emphasized the importance of unifying image understanding and image generation within a single framework. Early works such as Chameleon [28], Show-o [38], Transfusion [50], and Janus [35] adopt discrete visual representations and treat visual synthesis as autoregressive token prediction, where images are quantized into discrete tokens analogous to text, enabling LLMs to interpret and generate visual content in a unified token space. More recent models, including Metamorph [29] and the BLIP-3o family [2, 3], integrate autoregressive generation with diffusion-based continuous decoding, often relying on additional visual encoders such as CLIP [26] or SigLIP [41] to enhance visual understanding. In contrast to these general-purpose unified models, our work advances this paradigm in the autonomous driving domain by jointly predicting future frames and planning trajectories within a single VLM-based world model.

Vision–Language–Action Models. Recently, large vision–language–action (VLA) models have emerged as powerful frameworks for embodied decision-making. Built upon pretrained multimodal large language models (MLLMs), these systems typically predict future actions

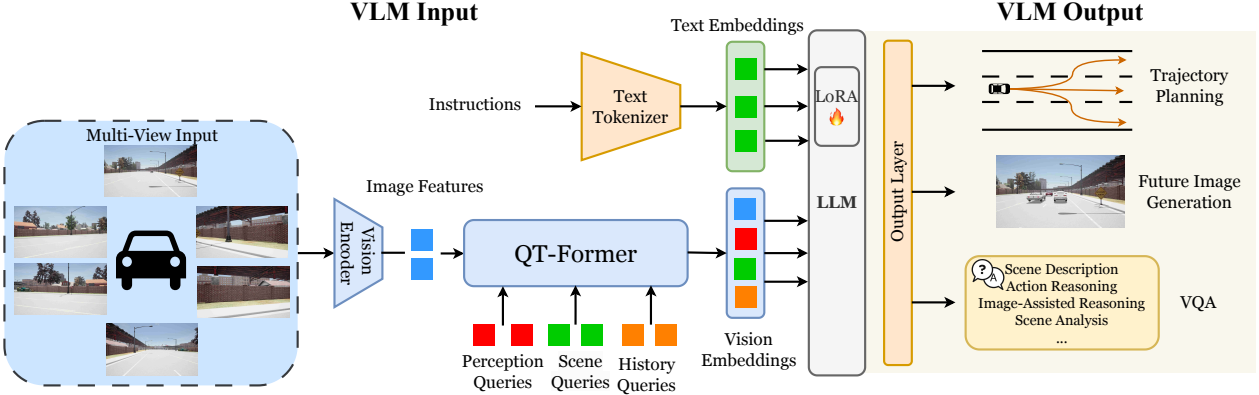


Figure 2. The pipeline of our UniDrive-WM Framework. The pipeline consists of: (1) a QT-Former based encoder to extract historical context and multi-view vision input; (2) The LLM for performing reasoning task and (3) The output layer generates the planning trajectory, future image prediction, which bridge the gaps between the planning space, image space and reasoning space. For the output layer, we provide detailed analysis in Fig. 3.

through either discrete action decoders [1, 19, 45] or continuous diffusion-based policy heads [10, 22]. By leveraging large-scale and diverse training corpora, MLLMs provide strong semantic grounding and generalization capabilities for downstream embodied tasks. In the autonomous driving setting, we treat ego-vehicle trajectories as the continuous action representation. Unlike standard manipulation or navigation environments, however, driving scenes are highly dynamic and visually complex, requiring the VLM to integrate richer contextual information—including temporal history, perception features, and multi-view observations to generate reliable and scene-consistent trajectory plans.

In this section, we present our unified understanding, generation and planning framework for autonomous driving. The pipeline is shown in Fig. 2. We begin with the formulation of our method, followed by the detailed analysis of the system architecture. We then analyse the model architecture for planning and image generation task. For the image generation, we explore both (1) Autoregressive image generation in discrete visual representation and (2) Diffusion-based continuous visual representation, and discuss their performance and impact on autonomous driving tasks. The task is defined as jointly predicting the future scene state and planning trajectory:

$$\{\hat{s}_{t+n}, \hat{a}_{t:t+m}\} \sim P_\theta(s_{1:t}, a_{1:t-1}, l), \quad (1)$$

which can be further decomposed as:

$$\begin{aligned} \{\hat{a}_t, \dots, \hat{a}_{t+m}\} &\sim P_\theta(\{a_t, \dots, a_{t+m}\} | s_t, l), \\ \hat{s}_{t+n} &\sim P_\theta(s_{t+n} | s_t, \hat{a}_t, \dots, \hat{a}_{t+m}, l), \end{aligned} \quad (2)$$

where s_t represents the multi-modal state information at time t , including multi-view images, historical context, and perception features; the model predicts the future front-view

image \hat{I}_{t+n} as part of the future state \hat{s}_{t+n} , and a_{t+m} denotes the predicted trajectory waypoint at time $t + m$; l is the high-level language or instruction condition. The model therefore aims to jointly reason about the future world state and plan consistent trajectories under a unified vision–language world model.

2.1. Vision Language Model

The key component of world model is understanding the current state and predicting the future state. Therefore leveraging the Vision Language Model’s reasoning and understanding ability, UniDrive-WM understands the current scene and instruct the trajectory planner and image image generation. We build our model upon Orion [7], a VLM-based model for autonomous driving planning task.

Vision Encoder For the vision encoder, we adopt QT-Former used by previous methods [7]. Specifically, two set of learnable queries are processed through self-attention(SA) to exchange their information and interact with image features F_m with 3D positional encoding in the cross-attention module. After that the perception queries are fed into the multiple auxiliary heads for object detection, including the critical objects, lanes, traffic state and motion prediction of dynamic objects. Additionally, we use a set of history queries $Q_h \in \mathbb{R}^{(N_h \times C_q)}$ and memory bank $M \in \mathbb{R}^{(N_h \times n) \times C_q}$ to retrieve and store the past n frames historical information. The QT-Former is formulated as:

$$\begin{aligned} Q_h &= \text{CA}(Q_h, M + P_t, M + P_t) \\ \hat{Q}_h &= \text{CA}(Q_h, Q_s, Q_s) \end{aligned} \quad (3)$$

where P_t denotes the relative timestamp embedding. The updated history queries \hat{Q}_h are stored in the memory bank

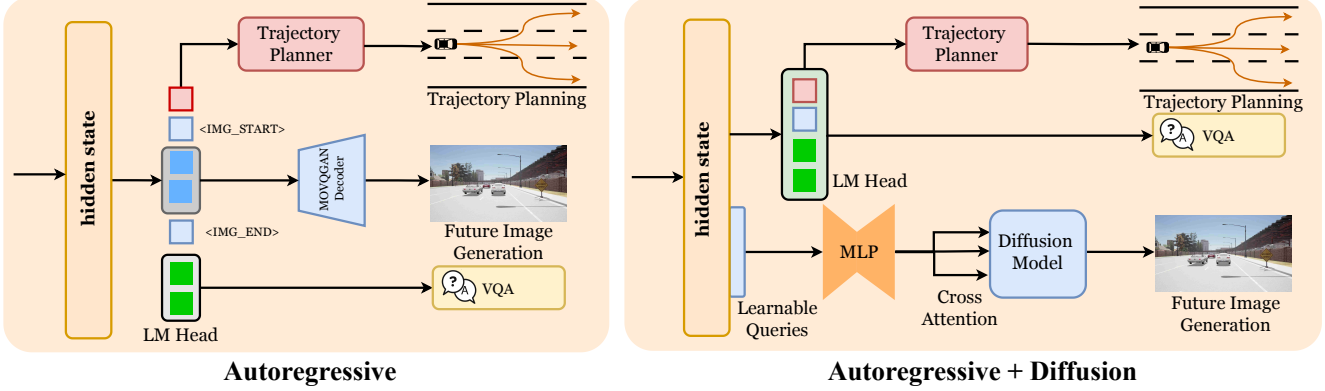


Figure 3. The two design choices for image generation in unified multimodal model. For the future image prediction, we use both Autoregressive and Autoregressive+Diffusion architecture. (a) Left: Autoregressive architecture; (b) Right: AR+Diffusion architecture.

M , formulated as

$$M = [\hat{Q}_h^{t-n}, \dots, \hat{Q}_h^{t-1}, \hat{Q}_h^t] \quad (4)$$

Finally, the two-layer Multi-layer Perceptron(MLP) is used to convert the updated history queries \hat{Q}_h and current scene features Q_s to history tokens x_h and scene tokens x_s in the reasoning space of LLM.

Large Language Model. The large language model (LLM) serves as the reasoning core of our framework, enabling text-based understanding and high-level reasoning tasks such as scene description, visual question answering, and action reasoning. We fine-tune the LLM using LoRA [12] to efficiently adapt it to domain-specific reasoning and instruction-following within autonomous driving scenarios.

2.2. Trajectory Planner

The trajectory planner establishes a differentiable connection between the semantic reasoning space of the VLM and the numerical action space of trajectory prediction through distribution learning in a latent space. We formulate trajectory generation as a conditional distribution problem, where the planner models a multi-modal distribution over future trajectories conditioned on high-level reasoning embeddings from the VLM:

$$p_\theta(\mathbf{a}_{t:t+m} | \mathbf{s}_t, \mathbf{h}_{\text{VLM}}), \quad (5)$$

where $\mathbf{a}_{t:t+m}$ denotes the predicted trajectory waypoints, \mathbf{s}_t represents the current state embedding, and \mathbf{h}_{VLM} denotes the high-level reasoning embedding (hidden representation) extracted from the VLM, which encodes the fused multi-view observations, temporal history, and textual instructions. A latent variable \mathbf{z}_a is introduced to capture the stochasticity of future motion in a Gaussian latent space,

and the planner learns to decode diverse yet semantically consistent trajectories from \mathbf{z}_a . In practice, we omit the explicit KL regularization term used in conventional VAE objectives, as we empirically find it may destabilize training in large-scale multimodal setups. This design provides a stable and differentiable bridge between language-based reasoning and continuous trajectory prediction.

2.3. Future Image Generation

As future frames naturally exist in autonomous driving datasets, we can utilize abundant video data to improve image generation quality. Inspired by recent advances in unifying image understanding and generation, we build the world model for autonomous driving. Here we adopt two different image generation architectures for future image prediction, as illustrated in Fig. 3. We discuss the design choices involved in building the understanding, planning, and image generation modules within a unified VLM framework, and analyze their impact on planning performance.

Formally, the future image prediction task can be formulated as:

$$p_\theta(\hat{\mathbf{I}}_{t+n} | \mathbf{s}_t, \mathbf{h}_{\text{VLM}}), \quad (6)$$

where \mathbf{s}_t denotes the multi-modal state information (including multi-view observations, temporal history, and perception features), and \mathbf{h}_{VLM} is the high-level reasoning embedding extracted from the VLM that encodes both visual and textual context. The model aims to predict the future front-view frame $\hat{\mathbf{I}}_{t+n}$ conditioned on these semantic representations. This unified probabilistic formulation covers both the discrete **autoregressive** decoder and the continuous **AR+Diffusion** decoder, which instantiate different parameterizations of the same conditional distribution $p_\theta(\cdot)$. We next describe the two decoding paradigms instantiated under this formulation.

Autoregressive Generation (Discrete Representation). As shown in Fig. 3(a), for the discrete image generation, we first activate the VLM’s visual generation ability by enlarging its codebook. Assume that the language–vision model uses a joint codebook $Z = Z_L + Z_I$. Through enlarging this codebook, the VLM can autoregressively perform multi-modal next-token prediction in both language and vision spaces. We introduce special tokens $\langle \text{image_start} \rangle$ and $\langle \text{image_end} \rangle$ to indicate the boundaries of visual token sequences and when to use the vision head. Specifically, based on the input visual tokens and the planning token $\mathbf{a}_{t:t+m}$, the model autoregressively performs next-token prediction, represented as:

$$P_\theta(q_{1:HW} | \mathbf{s}_t, \mathbf{a}_{t:t+m}) = \prod_{i=1}^{HW} P_\theta(q_i | q_{<i}, \mathbf{s}_t, \mathbf{a}_{t:t+m}), \quad (7)$$

where q_i are the visual tokens, \mathbf{s}_t represents the current multi-modal state (including visual observations, temporal history, and perception features), and $\mathbf{a}_{t:t+m}$ denotes the corresponding planning token that conditions the generation of subsequent visual tokens.

AR+Diffusion Generation(Continuous Representation). Apart from fully autoregressive generation, we also design an **Autoregressive + Diffusion** architecture for improved visual quality, as shown in Fig. 3(b).

The diffusion-based generation can be formulated as a conditional denoising process:

$$p_\theta(\hat{\mathbf{I}}_{t+n} | \mathbf{s}_t, \mathbf{h}_{\text{VLM}}), \quad (8)$$

where the decoder is conditioned on the high-level reasoning embedding \mathbf{h}_{VLM} and the latent image features produced by the autoregressive module. Starting from Gaussian noise $\mathbf{X}_0 \sim \mathcal{N}(0, 1)$, the diffusion process gradually refines \mathbf{X}_0 toward the latent embedding \mathbf{X}_1 of the ground-truth future image.

After extracting continuous visual embeddings, we employ an autoregressive transformer to generate corresponding latent image features conditioned on \mathbf{h}_{VLM} . Given an input instruction, the prompt is tokenized and mapped into a sequence of text embeddings $\mathbf{C} = [c_1, \dots, c_n]$ before the LM head. To enable visual latent inference, we append a learnable query token \mathbf{Q} to the sequence, where \mathbf{Q} is randomly initialized and updated throughout training. The transformer processes the combined sequence $[\mathbf{C}; \mathbf{Q}]$, during which \mathbf{Q} attends to the semantic context encoded in \mathbf{h}_{VLM} and aggregates features relevant for image synthesis. The output query token, denoted as \mathbf{Q}^* , serves as the predicted visual latent representation and is supervised to match the ground-truth image embedding \mathbf{X} extracted by the vision encoder. To align \mathbf{Q}^* with \mathbf{X} , we use a flow-

matching objective that models the continuous feature distribution. Given the ground-truth image feature \mathbf{X}_1 and the text-conditioned latent query \mathbf{Q} , we sample a timestep $t \sim \mathcal{U}(0, 1)$ and a noise vector $\mathbf{X}_0 \sim \mathcal{N}(0, 1)$. A latent point along the interpolation path is computed as

$$\mathbf{X}_t = t\mathbf{X}_1 + (1 - t)\mathbf{X}_0, \quad (9)$$

and the corresponding target velocity is

$$\mathbf{V}_t = \mathbf{X}_1 - \mathbf{X}_0. \quad (10)$$

The diffusion transformer predicts the velocity $\mathbf{V}_\theta(\mathbf{X}_t, \mathbf{Q}, t)$, and the flow-matching loss is

$$\mathcal{L}_{\text{FM}} = \mathbb{E} \left[\|\mathbf{V}_\theta(\mathbf{X}_t, \mathbf{Q}, t) - \mathbf{V}_t\|^2 \right]. \quad (11)$$

Notably, we freeze the vision encoder weights and fine-tune only the diffusion decoder. Although the decoder adopts a diffusion architecture, it is trained with a deterministic reconstruction loss rather than probabilistic sampling objectives. Consequently, during inference, the model performs deterministic reconstruction, which reduces diversity but ensures stable and accurate prediction of future frames in autonomous driving scenarios. We additionally apply CLIP-based supervision between the decoded future image and the ground-truth image to maintain semantic alignment:

$$\mathcal{L}_{\text{CLIP}} = 1 - \cos(E_{\text{clip}}(I_{\text{pred}}), E_{\text{clip}}(I_{\text{gt}})), \quad (12)$$

where $\cos(\mathbf{u}, \mathbf{v}) = \frac{\mathbf{u}^\top \mathbf{v}}{\|\mathbf{u}\| \|\mathbf{v}\|}$, $E_{\text{clip}}(\cdot)$ denotes the embedding produced by the CLIP image encoder, I_{pred} is the predicted image, and I_{gt} is the ground-truth image. This diffusion pathway complements the discrete autoregressive generation branch by providing a continuous, geometry-aware latent space for future frame synthesis, leading to stable and semantically consistent visual predictions within the unified world-model framework.

2.4. Joint Image Generation and Planning

To achieve joint image generation and planning, we place the planning token immediately before the image tokens, so that the generation of each image token is conditioned on the generated planning representation. In this way, image generation is jointly conditioned on the current-state visual embeddings and the predicted trajectory of the future state, enabling the synthesis of consistent future frames aligned with planned motion.

For the autoregressive generation, image token prediction is treated analogously to language generation and supervised through teacher-forcing with a cross-entropy loss. We adopt the pretrained QT-Former from ORION [7] and freeze its detection head during training. For the planning

Table 1. Closed-loop and Open-loop Results of E2E-AD Methods in Bench2Drive under base set. C/L refers to camera/LiDAR. Avg. L2 is averaged over the predictions in 2 seconds under 2Hz, similar to UniAD. * denote expert feature distillation. NC: navigation command, TP: target point, DS: Driving Score, SR: Success Rate.

Method	Condition	Modality	Closed-loop Metric				Open-loop Metric
			DS↑	SR(%)↑	Efficiency↑	Comfortness↑	
TCP* [36]	TP	C	40.70	15.00	54.26	47.80	1.70
TCP-ctrl*	TP	C	30.47	7.27	55.97	51.51	-
TCP-traj*	TP	C	59.90	30.00	76.54	18.08	1.70
TCP-traj w/o distillation	TP	C	49.30	20.45	78.78	22.96	1.96
ThinkTwice* [15]	TP	C	62.44	31.23	69.33	16.22	0.95
DriveAdapter* [14]	TP	C&L	64.22	33.08	70.22	16.01	1.01
AD-MLP [40]	NC	C	18.05	0.00	48.45	22.63	3.64
UniAD-Tiny [13]	NC	C	40.73	13.18	123.92	47.04	0.80
UniAD-Base [13]	NC	C	45.81	16.36	129.21	43.58	0.73
VAD [18]	NC	C	42.35	15.00	157.94	46.01	0.91
MomAD [27]	NC	C	44.54	16.71	170.21	48.63	0.87
GenAD [47]	NC	C	44.81	15.90	-	-	-
DriveTransformer-Large [17]	NC	C	63.46	35.01	100.64	20.78	0.62
ORION [7]	NC	C	77.74	54.62	151.48	17.38	0.68
Ours(AR)	NC	C	79.22	56.36	158.44	28.01	0.64

branch, following the implementations of VAD [18] and ORION [7], we train only the planning head with:

$$\mathcal{L}_{\text{plan}} = \mathcal{L}_{\text{col}} + \mathcal{L}_{\text{bd}} + \mathcal{L}_{\text{mse}}, \quad (13)$$

where \mathcal{L}_{col} denotes the collision loss, \mathcal{L}_{bd} the boundary loss, and \mathcal{L}_{mse} the mean squared error loss.

For the autoregressive architecture, the overall objective is represented as:

$$\mathcal{L} = \mathcal{L}_{\text{CE}} + \mathcal{L}_{\text{plan}}, \quad (14)$$

while for the autoregressive + diffusion architecture, where a learnable latent query in the latent space serves as the conditional embedding for image generation, the full objective becomes:

$$\mathcal{L} = \mathcal{L}_{\text{CE}} + \mathcal{L}_{\text{plan}} + \mathcal{L}_{\text{FM}} + \mathcal{L}_{\text{CLIP}}, \quad (15)$$

where \mathcal{L}_{FM} is the flow-matching loss and $\mathcal{L}_{\text{CLIP}}$ is the CLIP-based semantic alignment loss.

3. Experiments

3.1. Training Details

We follow ORION [7] for the detection training setup and conduct all experiments on 8×NVIDIA H200 GPUs. Following Omnidrive [31], we use EVA-02-L [6] as the vision encoder and adopt Vicuna 1.5 [46] as the base LLM, fine-tuned with LoRA (rank=16, $\alpha=16$). The numbers of scene, perception, and history queries are set to 512, 600, and 16, respectively, with a memory bank size of 16 frames.

Input images are augmented and resized to 640×640 . For future frame prediction, we use a 192×128 resolution for the autoregressive branch and 256×256 for the AR+Diffusion branch to balance quality and speed. The diffusion decoder uses 64 latent learnable query tokens. Additional hyperparameters and implementation details are provided in the Appendix.

3.2. Dataset

We train and evaluate UniDrive-WM on the Bench2Drive dataset [16], a closed-loop benchmark built on CARLA v2 [5]. Following prior work, we use the base split of 1000 driving scenes: 950 for training and 50 for open-loop validation. Each scene covers roughly 150 m of continuous driving in a distinct traffic scenario. For closed-loop evaluation, we follow the official protocol consisting of 220 short routes spanning 44 interactive scenarios (five routes per scenario).

3.3. Training Pipeline

To enable planning and image generation while preserving the VQA capability of the underlying VLM, we adopt a two-stage training strategy.

Stage 1: Joint Planning and Image Generation. We train the full model end-to-end, with the LLM updated via LoRA. For the autoregressive generator, the image-start token is placed immediately after the planning token to enforce planning-conditioned autoregressive decoding. For the AR+Diffusion architecture, the 64 learnable latent query

Table 2. Open-Loop Planning and perception metrics on Bench2Drive. Lower is better for planning errors, higher is better for mAP/NDS.

Method	L2 (m)↓			Box + Collision↓			mAP↑	mATE↓	mASE↓	mAOE↓	mAVE↓	NDS↑
	1s	2s	3s	1s	2s	3s						
BEVFormer [23]	—	—	—	—	—	—	0.616	0.372	0.079	0.044	0.808	0.642
UniAD [13]	0.521	1.265	2.140	0.0077	0.0387	0.0791	0.121	0.518	0.170	0.096	0.977	0.316
VAD [18]	0.454	0.912	1.477	0.00102	0.00202	0.00296	0.509	0.385	0.0854	0.0308	0.594	0.604
Orion [7]	0.268	0.631	1.129	0.00213	0.00467	0.00743	0.646	0.366	0.0765	0.0271	0.258	0.723
Ours(AR)	0.247	0.598	1.079	0.00198	0.00435	0.00668	0.663	0.335	0.0740	0.0262	0.249	0.746
Ours(AR+Diffusion)	0.251	0.608	1.092	0.00202	0.00441	0.00702	0.670	0.332	0.0736	0.0258	0.247	0.752

tokens are appended after the planning features in the latent space to condition the diffusion decoder.

Stage 2: Joint Planning, Image Generation, and VQA. We continue training with mixed VQA and driving data while keeping the same architectural setup as Stage 1. This stage reinforces the alignment of the vision–language–planning space by jointly optimizing VQA, trajectory planning, and future image prediction, enabling unified multimodal reasoning within a single framework.

3.4. Evaluation Metrics

For closed-loop evaluation, we follow the evaluation pipeline of Bench2Drive [16], which adopts four key metrics: Driving Score (DS), Success Rate (SR), Efficiency, Comfortness. The Success Rate measures the percentage of routes successfully completed within the designated time limit. The Driving Score follows the CARLA [5] protocol, combining route completion and violation penalties—where infractions proportionally reduce the score through discount factors. Efficiency and Comfortness respectively assess the speed performance and ride smoothness of the autonomous driving policy throughout the episode.

For open-loop evaluation, we report the L2 trajectory error and collision rate. We also evaluate the 3D detection performance using standard nuScenes metrics, including mAP, mATE, mASE, mAOE, mAVE, and NDS, which respectively measure detection accuracy, translation error, scale error, orientation error, velocity error, and the overall detection quality. For future frame prediction, we use the Fréchet Inception Distance (FID) to evaluate how closely the distribution of the generated frames matches that of the real future frames.

3.5. Evaluation of Trajectory Planning Results

We evaluate our results on the base validation set of Bench2Drive. We both report the open-loop and close-loop evaluation results. As shown in Tab. 1, for close-loop evaluation results, our method outperforms all the other methods that relies on target point and navigation command as conditions. Results show that our method achieves better

performance compared with previous end-to-end methods and VLM-guided planning methods, which demonstrates the effectiveness of image generation modality in boosting the performance of planning task.

We also evaluate the open-loop performance on Bench2Drive in Tab. 2. Notably, UniAD [13] computes L2 metrics and collision rate at each timestep, whereas VAD [18] and ORION [7] considers the average of all previous time-steps. We follow the evaluation method of VAD and ORION to evaluate our performance. Compared with previous methods that either purely do VLM-guided planning and end-to-end planning methods, our unified method achieves better performance on both the planning and detection tasks, which shows the effectiveness of future image prediction in improving the performance of the planning task.

3.6. Evaluation of Image Generation Results

We evaluate UniDrive-WM on both the autoregressive and AR+Diffusion image generation branches. Qualitative results are shown in Fig. 4, and quantitative results are provided in Tab. 3. Across both settings, our method produces visually coherent future frames that closely match the ground-truth scene evolution and remain consistent with the predicted trajectory. These properties translate into competitive or superior image generation quality, as reflected by low FID scores.

A particularly relevant comparison is FSDrive [39], a recent unified vision–planning framework that conditions planning on image features. Unlike FSDrive, our approach conditions image generation directly on the planning tokens, enabling planning-conditioned future frame prediction in both the AR and AR+Diffusion branches. This tighter coupling between planning and visual prediction improves trajectory alignment and yields future frames that more accurately follow the intended motion, contributing to our improved FID performance.

Analysis of Image Generation Methods. We compare the discrete autoregressive (AR) and continuous AR+Diffusion paradigms within our unified framework. Due to its sampling-based formulation, the diffusion de-

Table 3. Future frames generation results on the Bench2Drive [16] dataset. AR: Autoregressive. Lower FID indicates better visual fidelity.

Method	DriveGAN [20] [CVPR21]	DriveDreamer [32] [ECCV24]	Drive-WM [33] [CVPR24]	GEM [9] [CVPR25]	Doe-1 [48] [arxiv24]	FSDrive [39]	Ours(AR)	Ours (AR+Diffusion)
Type	GAN	Diffusion	Diffusion	Diffusion	AR	AR	AR	AR+Diffusion
FID ↓	62.3	42.8	17.8	13.2	18.6	9.3	6.4	7.1

Table 4. Ablation study about detection head, planning head, and image generation module for our AR architecture on Bench2Drive [16].

Detection head	Planning head	Image Gen.	L2 (m)↓			Box + Collision↓			mAP↑	mATE↓	mASE↓	mAOE↓	mAVE↓	NDS↑
			1s	2s	3s	1s	2s	3s						
✓	✓	✓	0.482	1.135	2.146	0.00387	0.00898	0.0177	—	—	—	—	—	—
✓	✓	✓	—	—	—	—	—	—	0.638	0.336	0.0726	0.0289	0.283	0.718
✓	✓	✓	0.269	0.632	1.130	0.00214	0.00469	0.00746	0.642	0.367	0.0767	0.0274	0.258	0.721
✓	✓	✓	0.247	0.598	1.079	0.00198	0.00435	0.00668	0.663	0.335	0.0740	0.0262	0.249	0.746

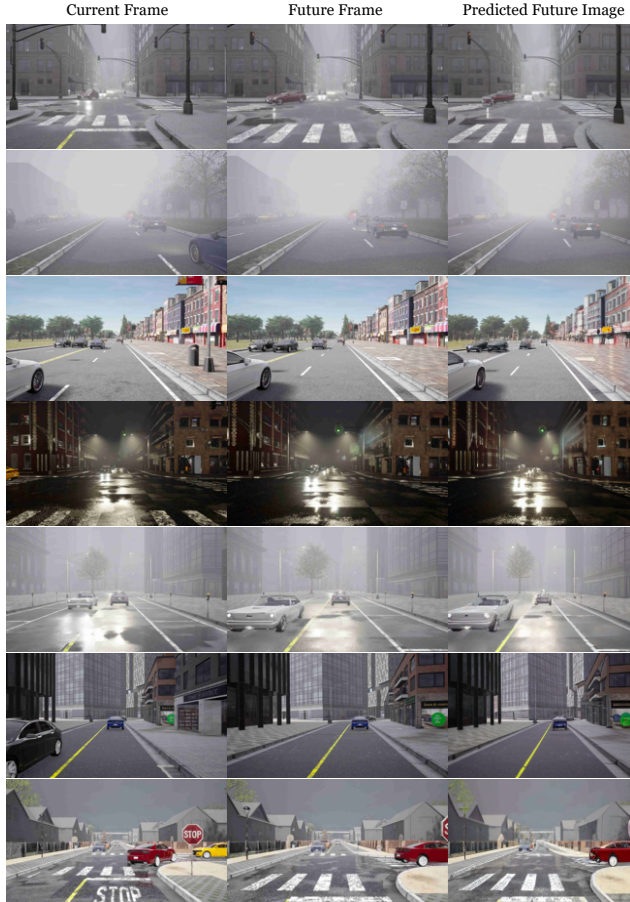


Figure 4. Visualization about autoregressive future image prediction results. Left: Current frame; Middle: Future frame; Right: Predicted future image.

coder exhibits higher variance than the AR approach. However, AR generation is fundamentally constrained by the number of image tokens: increasing the image resolu-

tion requires inserting more tokens, which substantially slows training and adaptation of the VLM. In contrast, the AR+Diffusion architecture operates in a continuous latent space, where feature alignment is independent of image resolution, enabling higher-fidelity future frame prediction.

Overall, these two pathways offer complementary trade-offs. The AR branch provides real-time generation and fast decision-making due to its discrete token-based design, but its representational capacity is limited by token granularity. The AR+Diffusion branch leverages continuous embeddings and learnable latent queries, yielding superior performance on visually complex or reasoning-intensive scenes. Its continuous latent representation enables more flexible conditioning and improves reconstruction fidelity in future frame prediction.

3.7. Ablation Study

We ablate the detection supervision and the image generation module to assess their contributions to planning, shown in Tab. 4. Removing the image generation head noticeably degrades trajectory accuracy and increases collision cases, indicating that future frame prediction provides useful auxiliary signals for planning. Disabling detection supervision further harms planning performance by weakening perception quality. Together, these findings show that both perception and future frame prediction play complementary roles, and that jointly optimizing all components within a unified world model yields more reliable driving behavior.

4. Conclusion and Future Works

We presented UniDrive-WM, a unified framework that integrates scene understanding, trajectory planning, and visual generation into a single world-model–driven pipeline. Leveraging a vision–language model (VLM) as the backbone, our method predicts future image frames from current and historical multi-view observations together with the planning tokens, and the planning-conditioned visual

predictions in turn enhance trajectory planning by providing a visual forecast of the expected future scene. Experimental results demonstrate that our approach not only achieves high-fidelity, planning-conditioned image generation, but also yields significant gains in planning accuracy and collision reduction. By conditioning the VLM on rich multi-view inputs, temporal history, and perception features, UniDrive-WM establishes a coherent bridge between reasoning, action, and visual imagination. Looking ahead, we plan to extend the framework to more interactive and long-horizon driving scenarios, paving the way toward next-generation world models for autonomous driving.

References

- [1] Jun Cen, Chaohui Yu, Hangjie Yuan, Yuming Jiang, Siteng Huang, Jiayan Guo, Xin Li, Yibing Song, Hao Luo, Fan Wang, et al. Worldvla: Towards autoregressive action world model. *arXiv preprint arXiv:2506.21539*, 2025. [3](#)
- [2] Juhai Chen, Zhiyang Xu, Xichen Pan, Yushi Hu, Can Qin, Tom Goldstein, Lifu Huang, Tianyi Zhou, Saining Xie, Silvio Savarese, Le Xue, Caiming Xiong, and Ran Xu. Blip3-o: A family of fully open unified multimodal models-architecture, training and dataset, 2025. [2](#)
- [3] Juhai Chen, Le Xue, Zhiyang Xu, Xichen Pan, Shusheng Yang, Can Qin, An Yan, Honglu Zhou, Zeyuan Chen, Lifu Huang, et al. Blip3o-next: Next frontier of native image generation. *arXiv preprint arXiv:2510.15857*, 2025. [2](#)
- [4] Ethan Chern, Zhulin Hu, Steffi Chern, Siqi Kou, Jiadi Su, Yan Ma, Zhijie Deng, and Pengfei Liu. Thinking with generated images. *arXiv preprint arXiv:2505.22525*, 2025. [1](#)
- [5] Alexey Dosovitskiy, German Ros, Felipe Codevilla, Antonio Lopez, and Vladlen Koltun. Carla: An open urban driving simulator. In *Conference on robot learning*, pages 1–16. PMLR, 2017. [6](#), [7](#)
- [6] Yuxin Fang, Quan Sun, Xinggang Wang, Tiejun Huang, Xinglong Wang, and Yue Cao. Eva-02: A visual representation for neon genesis. *Image and Vision Computing*, 149:105171, 2024. [6](#)
- [7] Haoyu Fu, Diankun Zhang, Zongchuang Zhao, Jianfeng Cui, Dingkang Liang, Chong Zhang, Dingyuan Zhang, Hongwei Xie, Bing Wang, and Xiang Bai. Orion: A holistic end-to-end autonomous driving framework by vision-language instructed action generation. *arXiv preprint arXiv:2503.19755*, 2025. [2](#), [3](#), [5](#), [6](#), [7](#), [12](#), [13](#)
- [8] Shenyuan Gao, Jiazhi Yang, Li Chen, Kashyap Chitta, Yihang Qiu, Andreas Geiger, Jun Zhang, and Hongyang Li. Vista: A generalizable driving world model with high fidelity and versatile controllability. *Advances in Neural Information Processing Systems*, 37:91560–91596, 2024. [2](#)
- [9] Mariam Hassan, Sebastian Stapf, Ahmad Rahimi, Pedro Rezende, Yasaman Haghighi, David Brüggemann, Isinsu Katircioglu, Lin Zhang, Xiaoran Chen, Suman Saha, et al. Gem: A generalizable ego-vision multimodal world model for fine-grained ego-motion, object dynamics, and scene composition control. In *Proceedings of the Computer Vision and Pattern Recognition Conference*, pages 22404–22415, 2025. [2](#), [8](#)
- [10] Haoran He, Yang Zhang, Liang Lin, Zhongwen Xu, and Ling Pan. Pre-trained video generative models as world simulators. *arXiv preprint arXiv:2502.07825*, 2025. [3](#)
- [11] Anthony Hu, Lloyd Russell, Hudson Yeo, Zak Murez, George Fedoseev, Alex Kendall, Jamie Shotton, and Gianluca Corrado. Gaia-1: A generative world model for autonomous driving. *arXiv preprint arXiv:2309.17080*, 2023. [2](#)
- [12] Edward J Hu, Yelong Shen, Phillip Wallis, Zeyuan Allen-Zhu, Yuanzhi Li, Shean Wang, Lu Wang, Weizhu Chen, et al. Lora: Low-rank adaptation of large language models. *ICLR*, 1(2):3, 2022. [4](#)
- [13] Yihan Hu, Jiazhi Yang, Li Chen, Keyu Li, Chonghao Sima, Xizhou Zhu, Siqi Chai, Senyao Du, Tianwei Lin, Wenhui Wang, Lewei Lu, Xiaosong Jia, Qiang Liu, Jifeng Dai, Yu Qiao, and Hongyang Li. Planning-oriented autonomous driving. In *Proceedings of the IEEE/CVF Conference on Computer Vision and Pattern Recognition*, 2023. [6](#), [7](#), [13](#)
- [14] Xiaosong Jia, Yulu Gao, Li Chen, Junchi Yan, Patrick Langechuan Liu, and Hongyang Li. Driveadapter: Breaking the coupling barrier of perception and planning in end-to-end autonomous driving. In *ICCV*, 2023. [6](#), [13](#)
- [15] Xiaosong Jia, Penghao Wu, Li Chen, Jiangwei Xie, Conghui He, Junchi Yan, and Hongyang Li. Think twice before driving: Towards scalable decoders for end-to-end autonomous driving. In *Proceedings of the IEEE/CVF Conference on Computer Vision and Pattern Recognition (CVPR)*, pages 21983–21994, 2023. [6](#), [13](#)
- [16] Xiaosong Jia, Zhenjie Yang, Qifeng Li, Zhiyuan Zhang, and Junchi Yan. Bench2drive: Towards multi-ability benchmarking of closed-loop end-to-end autonomous driving. *Advances in Neural Information Processing Systems*, 37:819–844, 2024. [6](#), [7](#), [8](#), [12](#)
- [17] Xiaosong Jia, Junqi You, Zhiyuan Zhang, and Junchi Yan. Drivetransformer: Unified transformer for scalable end-to-end autonomous driving. *arXiv preprint arXiv:2503.07656*, 2025. [6](#), [13](#)
- [18] Bo Jiang, Shaoyu Chen, Qing Xu, Bencheng Liao, Jiajie Chen, Helong Zhou, Qian Zhang, Wenyu Liu, Chang Huang, and Xinggang Wang. Vad: Vectorized scene representation for efficient autonomous driving. *ICCV*, 2023. [6](#), [7](#), [13](#)
- [19] Moo Jin Kim, Karl Pertsch, Siddharth Karamcheti, Ted Xiao, Ashwin Balakrishna, Suraj Nair, Rafael Rafailov, Ethan Foster, Grace Lam, Pannag Sanketi, et al. Openvla: An open-source vision-language-action model. *arXiv preprint arXiv:2406.09246*, 2024. [3](#)
- [20] Seung Wook Kim, Jonah Philion, Antonio Torralba, and Sanja Fidler. Drivegan: Towards a controllable high-quality neural simulation. In *Proceedings of the IEEE/CVF Conference on Computer Vision and Pattern Recognition*, pages 5820–5829, 2021. [8](#)
- [21] Chengzu Li, Wenshan Wu, Huanyu Zhang, Yan Xia, Shaoguang Mao, Li Dong, Ivan Vulić, and Furu Wei. Imagine while reasoning in space: Multimodal visualization-of-thought. *arXiv preprint arXiv:2501.07542*, 2025. [1](#)

[22] Shuang Li, Yihuai Gao, Dorsa Sadigh, and Shuran Song. Unified video action model. *arXiv preprint arXiv:2503.00200*, 2025. 3

[23] Zhiqi Li, Wenhui Wang, Hongyang Li, Enze Xie, Chong-hao Sima, Tong Lu, Yu Qiao, and Jifeng Dai. Bevformer: Learning bird’s-eye-view representation from multi-camera images via spatiotemporal transformers. *arXiv preprint arXiv:2203.17270*, 2022. 7

[24] Yifan Liao, Zhen Sun, Xiaoyun Qiu, Zixiao Zhao, Wenbing Tang, Xinlei He, Xinhua Zheng, Tianwei Zhang, Xinyi Huang, and Xingshuo Han. Work zones challenge vlm trajectory planning: Toward mitigation and robust autonomous driving. *arXiv preprint arXiv:2510.02803*, 2025. 2

[25] Tianran Liu, Shengwen Zhao, and Nicholas Rhinehart. Towards foundational lidar world models with efficient latent flow matching. *arXiv preprint arXiv:2506.23434*, 2025. 1

[26] Alec Radford, Jong Wook Kim, Chris Hallacy, Aditya Ramesh, Gabriel Goh, Sandhini Agarwal, Girish Sastry, Amanda Askell, Pamela Mishkin, Jack Clark, et al. Learning transferable visual models from natural language supervision. In *International conference on machine learning*, pages 8748–8763. PMLR, 2021. 2

[27] Ziying Song, Caiyan Jia, Lin Liu, Hongyu Pan, Yongchang Zhang, Junming Wang, Xingyu Zhang, Shaoqing Xu, Lei Yang, and Yadan Luo. Don’t shake the wheel: Momentum-aware planning in end-to-end autonomous driving. In *Proceedings of the Computer Vision and Pattern Recognition Conference*, pages 22432–22441, 2025. 6

[28] Chameleon Team. Chameleon: Mixed-modal early-fusion foundation models. *arXiv preprint arXiv:2405.09818*, 2024. 2

[29] Shengbang Tong, David Fan, Jiachen Zhu, Yunyang Xiong, Xinlei Chen, Koustuv Sinha, Michael Rabbat, Yann LeCun, Saining Xie, and Zhuang Liu. Metamorph: Multimodal understanding and generation via instruction tuning. *arXiv preprint arXiv:2412.14164*, 2024. 2

[30] Lening Wang, Wenzhao Zheng, Yilong Ren, Han Jiang, Zhiyong Cui, Haiyang Yu, and Jiwen Lu. Occsora: 4d occupancy generation models as world simulators for autonomous driving. *arXiv preprint arXiv:2405.20337*, 2024. 2

[31] Shihao Wang, Zhiding Yu, Xiaohui Jiang, Shiyi Lan, Min Shi, Nadine Chang, Jan Kautz, Ying Li, and Jose M Alvarez. Omnidrive: A holistic vision-language dataset for autonomous driving with counterfactual reasoning. In *Proceedings of the Computer Vision and Pattern Recognition Conference*, pages 22442–22452, 2025. 6

[32] Xiaofeng Wang, Zheng Zhu, Guan Huang, Xinze Chen, Jia-gang Zhu, and Jiwen Lu. Drivedreamer: Towards real-world-driven world models for autonomous driving. *arXiv preprint arXiv:2309.09777*, 2023. 8

[33] Yuqi Wang, Jiawei He, Lue Fan, Hongxin Li, Yuntao Chen, and Zhaoxiang Zhang. Driving into the future: Multiview visual forecasting and planning with world model for autonomous driving. *arXiv preprint arXiv:2311.17918*, 2023. 8

[34] Julong Wei, Shanshuai Yuan, Pengfei Li, Qingda Hu, Zhongxue Gan, and Wenchao Ding. Occlama: An occupancy-language-action generative world model for autonomous driving. *arXiv preprint arXiv:2409.03272*, 2024. 2

[35] Chengyue Wu, Xiaokang Chen, Zhiyu Wu, Yiyang Ma, Xingchao Liu, Zizheng Pan, Wen Liu, Zhenda Xie, Xingkai Yu, Chong Ruan, et al. Janus: Decoupling visual encoding for unified multimodal understanding and generation. In *Proceedings of the Computer Vision and Pattern Recognition Conference*, pages 12966–12977, 2025. 2

[36] Penghao Wu, Xiaosong Jia, Li Chen, Junchi Yan, Hongyang Li, and Yu Qiao. Trajectory-guided control prediction for end-to-end autonomous driving: A simple yet strong baseline. *Advances in Neural Information Processing Systems*, 35:6119–6132, 2022. 6, 13

[37] Zehuan Wu, Jingcheng Ni, Xiaodong Wang, Yuxin Guo, Rui Chen, Lewei Lu, Jifeng Dai, and Yuwen Xiong. Holodrive: Holistic 2d-3d multi-modal street scene generation for autonomous driving. *arXiv preprint arXiv:2412.01407*, 2024. 2

[38] Jinheng Xie, Weijia Mao, Zechen Bai, David Junhao Zhang, Weihao Wang, Kevin Qinghong Lin, Yuchao Gu, Zhijie Chen, Zhenheng Yang, and Mike Zheng Shou. Show-o: One single transformer to unify multimodal understanding and generation. *arXiv preprint arXiv:2408.12528*, 2024. 2

[39] Shuang Zeng, Xinyuan Chang, Mengwei Xie, Xinran Liu, Yifan Bai, Zheng Pan, Mu Xu, and Xing Wei. Futuresight-drive: Thinking visually with spatio-temporal cot for autonomous driving. *arXiv preprint arXiv:2505.17685*, 2025. 1, 7, 8

[40] Jiang-Tian Zhai, Ze Feng, Jinhao Du, Yongqiang Mao, Jiang-Jiang Liu, Zichang Tan, Yifu Zhang, Xiaoqing Ye, and Jingdong Wang. Rethinking the open-loop evaluation of end-to-end autonomous driving in nuscenes. *arXiv preprint arXiv:2305.10430*, 2023. 6, 13

[41] Xiaohua Zhai, Basil Mustafa, Alexander Kolesnikov, and Lucas Beyer. Sigmoid loss for language image pre-training. In *Proceedings of the IEEE/CVF international conference on computer vision*, pages 11975–11986, 2023. 2

[42] Kaiwen Zhang, Zhenyu Tang, Xiaotao Hu, Xingang Pan, Xiaoyang Guo, Yuan Liu, Jingwei Huang, Li Yuan, Qian Zhang, Xiao-Xiao Long, et al. Epona: Autoregressive diffusion world model for autonomous driving. *arXiv preprint arXiv:2506.24113*, 2025. 2

[43] Lunjun Zhang, Yuwen Xiong, Ze Yang, Sergio Casas, Rui Hu, and Raquel Urtasun. Copilot4d: Learning unsupervised world models for autonomous driving via discrete diffusion. *arXiv preprint arXiv:2311.01017*, 2023. 2

[44] Yumeng Zhang, Shi Gong, Kaixin Xiong, Xiaoqing Ye, Xiaofan Li, Xiao Tan, Fan Wang, Jizhou Huang, Hua Wu, and Haifeng Wang. Bevworld: A multimodal world simulator for autonomous driving via scene-level bev latents. *arXiv preprint arXiv:2407.05679*, 2024. 2

[45] Qingqing Zhao, Yao Lu, Moo Jin Kim, Zipeng Fu, Zhuoyang Zhang, Yecheng Wu, Zhaoshuo Li, Qianli Ma, Song Han, Chelsea Finn, et al. Cot-vla: Visual chain-of-thought reasoning for vision-language-action models. In *Proceedings of the Computer Vision and Pattern Recognition Conference*, pages 1702–1713, 2025. 3

- [46] Lianmin Zheng, Wei-Lin Chiang, Ying Sheng, Siyuan Zhuang, Zhanghao Wu, Yonghao Zhuang, Zi Lin, Zhuohan Li, Dacheng Li, Eric Xing, et al. Judging llm-as-a-judge with mt-bench and chatbot arena. *Advances in neural information processing systems*, 36:46595–46623, 2023. 6
- [47] Wenzhao Zheng, Ruiqi Song, Xianda Guo, Chenming Zhang, and Long Chen. Genad: Generative end-to-end autonomous driving. In *European Conference on Computer Vision*, pages 87–104. Springer, 2024. 6
- [48] Wenzhao Zheng, Zetian Xia, Yuanhui Huang, Sicheng Zuo, Jie Zhou, and Jiwen Lu. Doe-1: Closed-loop autonomous driving with large world model. *arXiv preprint arXiv:2412.09627*, 2024. 8
- [49] Yupeng Zheng, Pengxuan Yang, Zebin Xing, Qichao Zhang, Yuhang Zheng, Yinfeng Gao, Pengfei Li, Teng Zhang, Zhongpu Xia, Peng Jia, et al. World4drive: End-to-end autonomous driving via intention-aware physical latent world model. In *Proceedings of the IEEE/CVF International Conference on Computer Vision*, pages 28632–28642, 2025. 1
- [50] Chunting Zhou, Lili Yu, Arun Babu, Kushal Tirumala, Michihiro Yasunaga, Leonid Shamis, Jacob Kahn, Xuezhe Ma, Luke Zettlemoyer, and Omer Levy. Transfusion: Predict the next token and diffuse images with one multi-modal model. *arXiv preprint arXiv:2408.11039*, 2024. 2
- [51] Vlas Zyrianov, Henry Che, Zhijian Liu, and Shenlong Wang. Lidardm: Generative lidar simulation in a generated world. In *2025 IEEE International Conference on Robotics and Automation (ICRA)*, pages 6055–6062. IEEE, 2025. 2

UniDrive-WM: Unified Understanding, Planning and Generation World Model For Autonomous Driving

Supplementary Material

A. More Results

A.1. More Results about Close-Loop Evaluation

We add additional close-loop evaluation results about multi-ability on Bench2Drive in Tab 5. Compared with baseline methods, we achieve better performance in Merging, Overtaking, Emergency Brake, and Trafic Sign ability, which shows that benefiting from the VLM’s reasoning ability and the future image prediction ability, our method achieves better results on multi-ability, along with the Mean score.

A.2. Visualization of AR+Diffusion Future Image Prediction

We show additional visualization results of our AR+Diffusion architecture in Fig. 5. The results demonstrate the architecture’s ability to generate plausible future frames.

A.3. Further Comparison between AR and AR+Diffusion Architecture

We provide further comparison between our proposed AR architecture and AR+Diffusion architecture, shown in Tab. 6. Results show that the AR architecture shows slightly better results compared with AR+Diffusion architecture. We regard it as that the token-space insertion of image tokens provides a more explicit supervision for the planning compared with inserting learnable queries in hidden states. However, AR+Diffusion has the potential to generate higher-resolution outputs(512×512), offering superior generation quality. For AR-based architectures, increasing image resolution significantly increases the number of visual tokens, which in turn slows down convergence during training and speed during inference. For AR+Diffusion architecture, future works may be using discrete predicted image tokens as additional conditioning signals for the diffusion model to diffuse the final VAE features to further improve the planning performance.

A.4. Results on VQA

We report our Visual Question Answering (VQA) results in Tab. 7. We adopt standard natural language generation metrics for evaluation. CIDEr measures the semantic relevance between generated answers and human references using TF-IDF-weighted n-grams. BLEU evaluates n-gram precision to quantify lexical overlap, while ROUGE-L computes the longest common subsequence to capture sequence-level similarity and structural consistency.

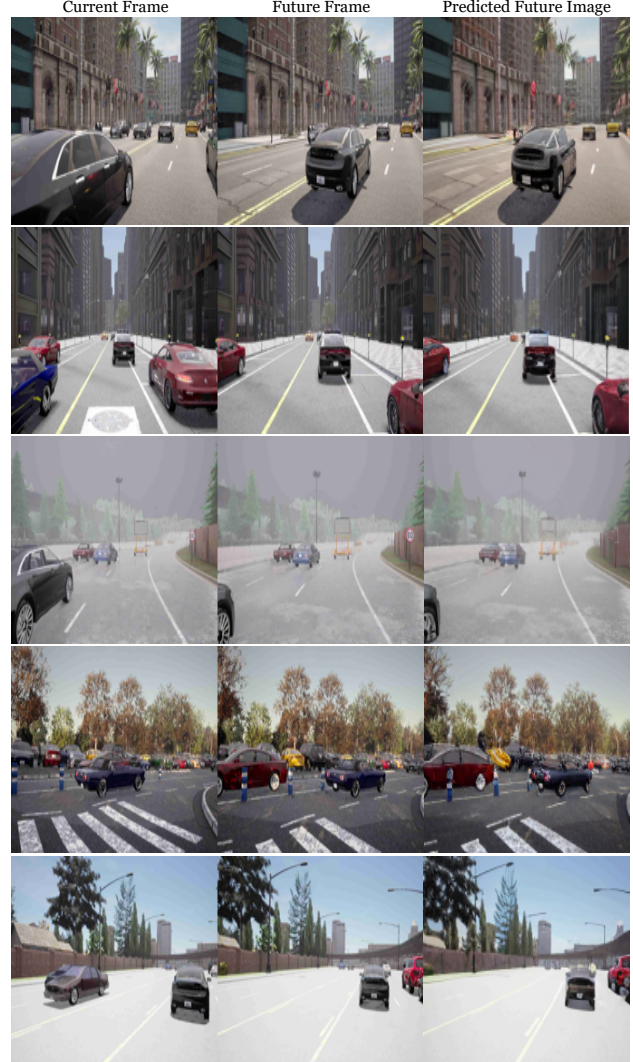


Figure 5. Visualization of AR+Diffusion result. Left: Current frame; Middle: Future frame; Right: Predicted future image.

We evaluate VQA performance on Bench2Drive [16] using the Chat-B2D QA annotations [7]. Compared with the model variant without the image-generation module, incorporating image generation consistently improves all VQA metrics. This indicates that the future frame prediction provides additional structural cues that benefit question answering. Intuitively, better modeling of future visual states enhances the model’s understanding of the current scene, which aligns with human perception. We also show the vi-

Table 5. Multi-Ability Results under Bench2Drive base set. * denote expert feature distillation. C/L refers to camera/LiDAR. NC: navigation command, TP: target point.

Method	Condition	Modality	Ability (%) ↑					
			Merging	Overtaking	Emergency Brake	Give Way	Traffic Sign	Mean
TCP* [36]	TP	C	16.18	20.00	20.00	10.00	6.99	14.63
TCP-ctrl*	TP	C	10.29	4.44	10.00	10.00	6.45	8.23
TCP-traj*	TP	C	8.89	24.29	51.67	40.00	46.28	34.22
TCP-traj w/o distillation	TP	C	17.14	6.67	40.00	50.00	28.72	28.51
ThinkTwice* [15]	TP	C	27.38	18.42	35.82	50.00	54.23	37.17
DriveAdapter* [14]	TP	C&L	28.82	26.38	48.76	50.00	56.43	42.08
AD-MLP [40]	NC	C	0.00	0.00	0.00	0.00	4.35	0.87
UniAD-Tiny [13]	NC	C	8.89	9.33	20.00	20.00	15.43	14.73
UniAD-Base [13]	NC	C	14.10	17.78	21.67	10.00	14.21	15.55
VAD [18]	NC	C	8.11	24.44	18.64	20.00	19.15	18.07
DriveTransformer-Large [17]	NC	C	17.57	35.00	48.36	40.00	52.10	38.60
ORION	NC	C	25.00	71.11	78.33	30.00	69.15	54.72
Ours(AR)	NC	C	29.81	74.04	79.84	40.00	71.30	59.01

Table 6. Further comparison about future image prediction result. DS and SR denote Driving Score and Success Rate separately.

Future Image Prediction	Closed-loop		Open-loop		Ability Average
	DS↑	SR(%)↑	Avg. L2 (m)↓	Avg. col(%)↓	
Ours(AR+Diffusion)	78.24	55.58	0.65	0.45	57.86
Ours(AR)	79.22	56.36	0.64	0.43	59.01

Table 7. Additional ablation about VQA score.

Image Generation	CIDEr ↑	BLEU ↑	ROUGE-L↑
-	65.7	52.4	77.5
✓	66.3	52.9	78.3

sualization of the VQA result in open-loop evaluation in Fig 6. These results demonstrate that our model not only comprehends the current scene, but also performs effective future-state reasoning, enabling it to produce reliable, decision-oriented answers even in complex driving scenarios and challenging weather conditions.

B. Additional Details on QT-Former

We follow ORION [7] and adopt a QT-Former as the perception backbone to bridge multi-view visual observations and downstream reasoning. The QT-Former operates with three types of learnable queries: scene queries, perception queries, and history queries, which together support spatial and temporal modeling in autonomous driving scenarios.

Scene and Perception Queries. We initialize learnable scene queries $Q_s \in \mathbb{R}^{N_s \times C_q}$ and perception queries $Q_p \in$

$\mathbb{R}^{N_p \times C_q}$, where N_s and N_p denote the numbers of scene and perception queries, respectively, and C_q is the query dimension. The scene queries are designed to capture global, holistic scene-level context such as road layout and traffic configuration, while the perception queries focus on object-centric representations for localized detection and motion estimation. Both types of queries interact with multi-view image features F_m and their associated 3D positional encodings P_m through cross-attention, enabling structured aggregation of spatial information.

The updated perception queries are passed to multiple auxiliary heads responsible for object detection (e.g., critical objects and lanes), traffic state estimation, and motion prediction for dynamic agents. We report 3D object detection performance using the outputs produced by the detection head.

History Queries. In addition to spatial perception, UniDrive-WM maintains a set of history queries to model temporal evolution across frames. The history queries act as a compact memory representation that aggregates information from past observations, allowing the model to reason over temporal context beyond a single frame. At each timestep, the current scene queries attend to the stored history queries via cross-attention, enabling selective re-

trieval and update of temporally relevant information. During unified training, the detection heads are frozen to preserve detection stability, while the scene, perception, and history queries remain trainable and are optimized jointly with the VLM backbone. This design provides a stable spatio-temporal perceptual interface for downstream planning and image generation, supporting UniDrive-WM’s unified world modeling.



Q1: "Could you describe the overall environment and objects captured in the images provided?"

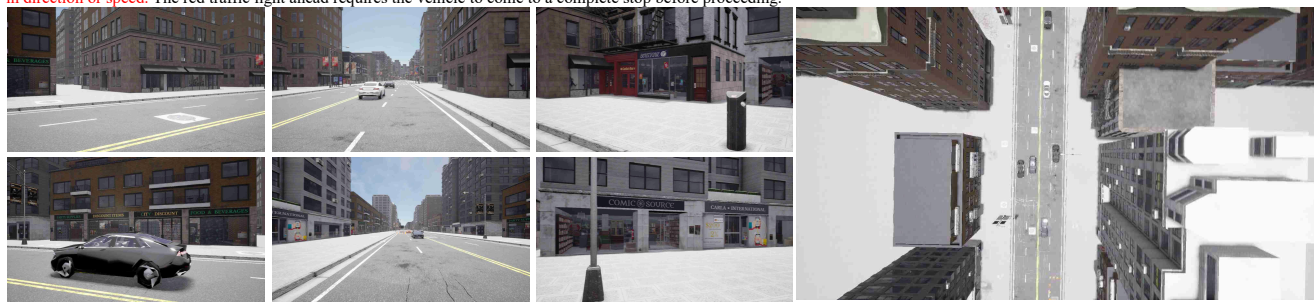
A1: "The scene depicts an intersection during what appears to be early evening or late afternoon, given the dark sky. The road is clear with no visible obstacles, and the traffic lights are showing red. There are no pedestrians or other vehicles in the immediate vicinity. The surroundings include a billboard, some trees, and a few buildings, suggesting a suburban setting. The road surface looks smooth and well-maintained."

Q2: "Which objects in the scene are critical, and what effects do they have on the ego vehicle's movement?"

A2: "Traffic light at <1.33, 24.63> showing red, indicating the need to stop."

Q3: "Please describe your driving behavior and explain the reasons."

A3: "You should keep and lanefollow. The decision to keep the current speed and follow the lane is influenced by the absence of any immediate obstacles or other vehicles requiring a change in direction or speed. The red traffic light ahead requires the vehicle to come to a complete stop before proceeding."



Q1: "Could you describe the overall environment and objects captured in the images provided?"

A1: "The scene depicts an urban street during daytime under clear weather conditions. The road is dry and well-maintained, with clearly marked lanes and a double yellow line dividing the opposing traffic directions. There are two vehicles ahead in the same lane as the ego vehicle, both traveling in the same direction. The traffic lights ahead are green, allowing for uninterrupted travel. The surrounding buildings are multi-story structures typical of a city environment, with storefronts and signage visible along the sidewalks."

Q2: "Which objects in the scene are critical, and what effects do they have on the ego vehicle's movement?"

A2: "Car at <2.52, 17.73> is 17.73 meters ahead and 2.52 meters to the left of the ego vehicle, moving at a similar speed, may influence lane choice."

Q3: "Please describe your driving behavior and explain the reasons."

A3: "You should maintain your current speed and follow the lane. The decision to maintain speed and follow the lane is influenced by the presence of the car ahead in the same lane, which is moving at a similar speed, suggesting a safe following distance. The green traffic light ahead indicates that there are no immediate stops required, allowing for continuous motion. The road conditions are favorable, with no visible obstacles or hazards."



Q1: "Could you describe the overall environment and objects captured in the images provided?"

A1: "The scene depicts a rainy highway with reduced visibility due to the weather conditions. The road surface appears wet, indicating recent or ongoing precipitation. A blue car is visible in the right lane, moving away from the viewer's perspective. The surrounding area includes a barrier on the right side and greenery beyond it, with overhead signs providing direction or exit information. The overall atmosphere suggests caution due to the slippery road conditions and limited visibility."

Q2: "Which objects in the scene are critical, and what effects do they have on the ego vehicle's movement?"

A2: "Blue car at <2.83, 24.21> in the right lane, moving at a speed of 5.44 m/s, heading away from the ego vehicle, and potentially influencing lane-changing decisions."

Q3: "Please describe your driving behavior and explain the reasons."

A3: "You should maintain your current speed and prepare to change lanes to the left. The decision to change lanes is influenced by the need to navigate around the blue car in the right lane, which is moving at a different speed and trajectory. The wet road conditions require careful maneuvering to avoid skidding or losing control during the lane change. Ensure there is sufficient space in the left lane before initiating the lane change to maintain safety."

Figure 6. Visualization of our VQA result on Bench2Drive open-loop evaluation. For each scene, we show the multi-view input images and the Bird's Eye View(BEV). The question-answer includes the model's understanding of the current state and reasoning about the ego vehicle's movement and driving behavior. Red text highlights our method's scene comprehension and reasoning.